Fourth-order dispersion mediated modulation instability in dispersion oscillating fibers

Fourth-order dispersion mediated modulation instability in dispersion oscillating fibers

Maxime Droques,[1] Alexandre Kudlinski,[1] Geraud Bouwmans,[1] Gilbert Martinelli,[1] Arnaud Mussot,[1,*] Andrea Armaroli,[2] and Fabio Biancalana[2,3]

[1]*Laboratoire PhLAM (UMR CNRS 8523), IRCICA (USR CNRS 3380), Université Lille 1, 59655 Villeneuve d'Ascq, France*

[2]*Max Planck Institute for the Science of Light, Günther-Scharowsky-Str. 1/Bau 24, 91058 Erlangen, Germany*

[3]*School of Engineering and Physical Sciences, Heriot-Watt University, EH14 4AS Edinburgh, UK*

**Corresponding author: arnaud.mussot@univ-lille1.fr*

Received June 3, 2013; revised July 23, 2013; accepted July 26, 2013;
posted July 26, 2013 (Doc. ID 191672); published August 30, 2013

We investigate the role played by fourth-order dispersion on the modulation instability process in dispersion oscillating fibers. It not only leads to the appearance of instability sidebands in the normal dispersion regime (as in uniform fibers), but also to a new class of large detuned instability peaks that we ascribe to the variation of dispersion. All these theoretical predictions are experimentally confirmed. © 2013 Optical Society of America

OCIS codes: (060.4370) Nonlinear optics, fibers; (190.4380) Nonlinear optics, four-wave mixing; (190.4410) Nonlinear optics, parametric processes.

http://dx.doi.org/10.1364/OL.38.003464

The modulation instability (MI) process in optical fibers involves the nonlinear interaction between an intense pump wave and a weak perturbation that grows exponentially. This phenomenon is conveniently described as a four-wave mixing process ruled by energy and momentum conservations. The latter condition requires phase matching, i.e., a compensation between linear and nonlinear phase mismatches due to group velocity dispersion (GVD) and Kerr nonlinearity, respectively. Only a negative contribution from dispersive effects permits compensation for the Kerr nonlinear phase mismatch always being positive in glass fibers. In single mode optical fibers, limiting our investigations to a scalar configuration, it seems natural to launch the pump field in the anomalous dispersion region in order to obtain a perfect phase matching. However, MI can also occur in the normal GVD regime, due to negative fourth-order dispersion (FOD) in uniform fibers [1,2], to periodic boundary conditions in fiber cavities [3], or to a periodic variation of the wave vector mismatch. The latter process can be obtained from periodically varying power [4,5] or dispersion [6–8] causing the appearance of a virtual grating, the wave vector of which contributes to the phase matching relation. This has been widely theoretically investigated in the context of long-haul telecommunication networks [4–7,9] because this effect is highly detrimental in such settings. In fact, due to the spatial scale (in the order of a hundred kilometer) involved in these systems, MI sidebands are spectrally generated in the tens of GHz range, that typically corresponds to the bit rate of modern telecommunication systems and then leads to signal distortions.

Very recently, technical progress in the manufacturing of photonic crystal fiber (PCF) has allowed for the fabrication of periodically tapered PCFs with periods in the meter range [8,10]. In such dispersion oscillating fibers (DOFs), MI sidebands are generated in the THz range. While previous work did not reveal any significant impact of higher-order dispersion on the MI process in DOFs, it is expected to play an important role under specific conditions, e.g., in the proximity of zero-dispersion wavelength (ZDW) at high input power, as in uniform fibers [1,2]. In this work, we investigate the impact of FOD on the MI process in DOFs. We show that the combined effect of this higher-order dispersion term and of axially periodic dispersion leads to the appearance of new MI peaks that are experimentally observed.

The MI process in optical fiber systems with longitudinal periodicity can be described using the Floquet theory [11–13] or, more simply, using quasi-phase-matching (QPM) arguments [5,7,11,14], in analogy with QPM in poled second-order nonlinear materials. Considering dispersion terms up to the fourth-order, the use of Floquet theory and the method of averaging results in the following parametric resonance condition [13,15]:

$$\left(\frac{\bar{\beta}_2\Omega_k^2}{2}+\frac{\bar{\beta}_4}{24}\Omega_k^4\right)\left(\frac{\bar{\beta}_2\Omega_k^2}{2}+\frac{\bar{\beta}_4}{24}\Omega_k^4+2\gamma P\right)=\left[\frac{\pi m}{Z}\right]^2, \quad (1)$$

where m is a non-negative integer, Ω_k is the pulsation detuning from the pump, $\bar{\beta}_2$ and $\bar{\beta}_4$ are the average second-order and FOD terms, γ is the average nonlinear coefficient of the fiber, and P is the pump peak power. It is worth noting that if the period of oscillation of the GVD is short compared to the nonlinear length [$L_{\mathrm{NL}}=(\gamma P)^{-1}$], or at least of the same order, i.e., $Z<\pi L_{\mathrm{NL}}$, we can use the approximate QPM relation, which provides a clearer picture of the physical mechanisms. In all this work this condition is fulfilled ($L_{\mathrm{NL}}=0.33$ m and $Z=1$ m), so we will then use the QPM approach. We remind that, in periodic fiber systems, QPM is achieved if the phase mismatch integrated over one period is an integer multiple of 2π [11,14], i.e.,

$$\bar{\beta}_2\Omega_k^2+\frac{\bar{\beta}_4}{12}\Omega_k^4+2\gamma P=\frac{2\pi k}{Z}, \quad (2)$$

where k is a positive or negative integer. Equation (2) is strictly rigorous for $k=0$, while it is an approximation otherwise. Interestingly, for each parametric resonance order m in Eq. (1), there is a one-to-one correspondence

between the exact and the approximated relations, i.e., for each $m = |k| \neq 0$ we can find a solution of the QPM condition.

From Eq. (2), it is straightforward to show that QPM is achieved for pulsations:

$$\Omega_k = \pm\sqrt{-\frac{6\bar{\beta}_2}{\bar{\beta}_4} \pm 2\sqrt{9\frac{\bar{\beta}_2{}^2}{\bar{\beta}_4{}^2} + \frac{3}{\bar{\beta}_4}\left(\frac{2\pi k}{Z} - 2\gamma P\right)}}. \quad (3)$$

In the following, we will focus our attention on negative FOD, i.e., $\bar{\beta}_4 < 0$, as occurs in most optical fibers with a single zero dispersion wavelength. Figure 1 shows QPM curves obtained from Eq. (3), with $Z = 1$ m, $\bar{\beta}_4 = -1.1 \times 10^{-7}$ ps^4/m, $P = 40$ W and $\gamma = 7.5\,\mathrm{W}^{-1}\cdot\mathrm{km}^{-1}$. Note that these parameters correspond to the ones of the experiment described below. Solid blue lines have been plotted by taking the $\bar{\beta}_4$ term of Eq. (3) into account, while this term has been neglected for the red dashed lines. In this graph, $k = 0$ lines correspond to solutions that would be obtained in a uniform fiber, while $k \neq 0$ solutions directly arise from the oscillating nature of dispersion. For the sake of clarity, we limit our representation to $k = \pm 1$ since they summarize the new dynamics of the process, and other k values lead to similar behaviors. Two main features related to the inclusion of the FOD term in the QPM relation can be observed from Fig. 1. First, for $k \leq 0$, solutions are found in both the normal and anomalous dispersion regimes, while they only exist in anomalous dispersion when $\bar{\beta}_4$ is neglected. This phenomenon is analogous to the MI process assisted by FOD in uniform fibers (i.e., for $k = 0$) in which the negative FOD term contributes to the linear phase mismatch to compensate for the positive nonlinear one [1,2]. Second, QPM curves obtained for $k > 0$ values exhibit two branches, i.e., two solutions are found for a fixed $\bar{\beta}_2$, while only one is expected when $\bar{\beta}_4$ is neglected. The solution with the largest shift from the pump on each branch is directly linked to the presence of the $\bar{\beta}_4$ term and only exits for $\bar{\beta}_2$ values larger than $\sqrt{(\bar{\beta}_4/3)(2\gamma P - (2\pi k/Z))}$.

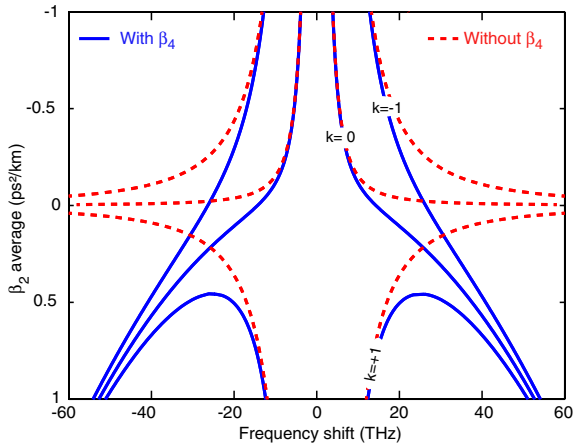

Fig. 1. Quasi-phase matching curves calculated from Eq. (3) with and without the $\bar{\beta}_4$ term (blue solid and red dashed lines, respectively) as a function of average GVD for a period $Z = 1$ m.

Before attempting an experimental demonstration of FOD-mediated MI, we investigated the impact of the modulation period on the process in order to understand why these specific features were not observed in our previous experiments performed with a modulation period of 10 m [8,10]. Figure 2(a) shows the evolution of the gain spectrum versus modulation period Z. These numerical simulations have been obtained by using the method described in [16] for $\bar{\beta}_2 = +0.49$ ps^2/km. Other parameters are similar to those used in this work. This figure shows that the gain of the second branch (with the largest detuning) indeed strongly depends on the modulation period. For the sake of clarity, Fig. 2(b) shows a close-up on the $k = 1$ MI sideband which has furthermore been recentered around its central frequency given by Eq. (3). First of all, we see that the gain oscillates versus the modulation period. This behavior has already been described in [10] and more details on these dynamics can be found in this reference. However, what we would like to show with these figures is the decrease of both the gain band and the maximum gain for increasing modulation periods. For instance, with $Z = 1$ m the gain is 25 dB, while it falls down to 4 dB for $Z = 10$ m. It is thus likely that in our previous experiments performed for a modulation period of 10 m, the gain of this second solution was too low and it was furthermore affected by detrimental longitudinal fluctuations, which are known to strongly reduce the efficiency of the parametric processes in optical fibers [17].

In order to experimentally highlight the role played by FOD, we therefore fabricated a DOF with a shorter longitudinal modulation period than the one used in our previous experiments (1 m versus 10 m). The dispersion map has a sine shape and a modulation amplitude of $\pm 6\%$, which corresponds to total variations of the zero dispersion wavelength of about 10 nm. At 1059 nm, $\bar{\beta}_2 = 0$ and β_2 oscillates between ± 1.1 ps^2/km, the group birefringence is 1.3×10^{-4} so that the DOF can be

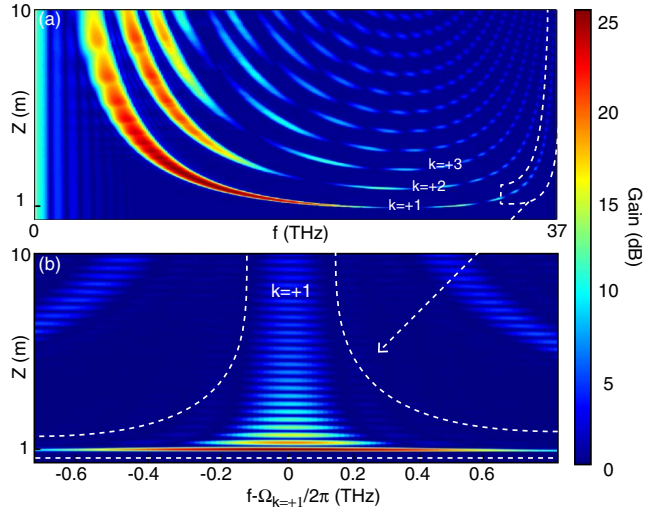

Fig. 2. (a) Gain spectrum versus modulation period. (b) Close-up of the evolution of the second solution of the MI sidelobe, corresponding to $q = 1$, as a function of the modulation period Z. The sidelobe is centered around its central frequency for every Z. The whole spectrum is in the inset on the right.

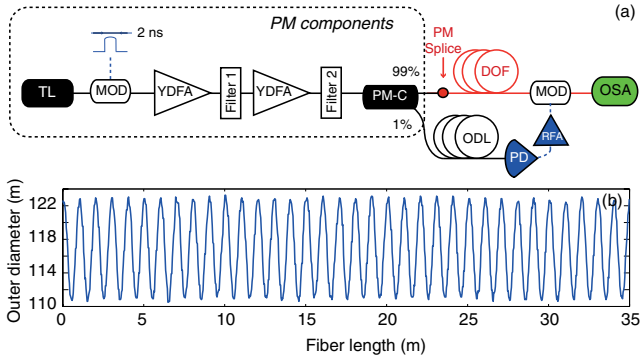

Fig. 3. (a) Scheme of the experimental setup and (b) longitudinal evolution of the outer diameter.

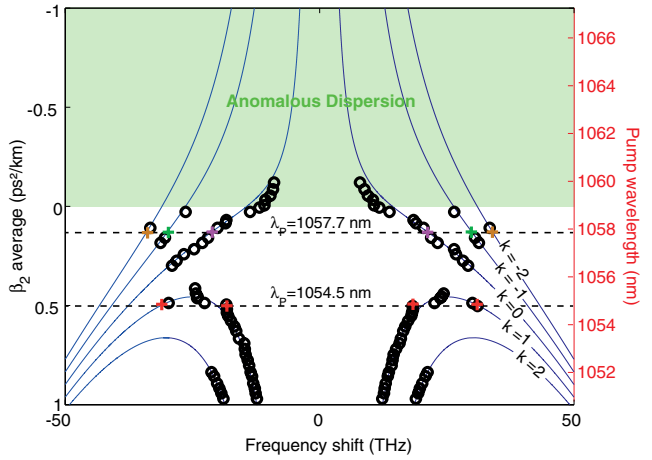

Fig. 4. QPM curves calculated from Eq. (2) (solid line) and measurement of MI sideband frequencies done by tuning the pump wavelength (markers). Crosses highlight frequencies appearing in the experimental spectra shown in Figs. 5(a) and 5(b).

considered as polarization maintaining (PM), and the linear attenuation is 8 dB/km. The experimental setup is schematized in Fig. 3(a). The pump system is made of a continuous-wave tunable laser (TL) diode that is sent into an intensity modulator (MOD) in order to shape 2 ns square pulses at 1 MHz repetition rate. They are amplified by two Ytterbium-doped fiber amplifiers (YDFAs) at the output of which two successive tunable filters are inserted to remove the excess amplified spontaneous emission (ASE) around the pump. It is finally launched into the PCF with a 99/1 coupler. All of these components are PM so that the linear polarization state can be aligned to a principal axis of the DOF in order to limit our investigations to a scalar MI process. Additionally, 1% of the input pump beam is sent to a photodiode (PD) whose output electrical signal is amplified and used to drive a second intensity modulator in order to remove residual ASE between the 2 ns pump pulses. The synchronization of the modulator to the pulse train is done with an optical delay line (ODL) made of a standard optical fiber with an optimized length. This improvement of the detection leads to a lowering of the noise background by about 8 dB on the optical spectrum analyzer, which proved to be critical to experimentally observe $\bar{\beta}_4$ mediated MI sidebands.

Experiments were performed in the DOF described above, the outer diameter evolution of which is represented in Fig. 3(b) (longitudinal period of 1 m) for a fixed pump peak power of 40 W and total fiber length of 35 m. The adjustment of the $\bar{\beta}_2$ value was simply done by tuning the wavelength of the pump laser. By doing so in the normal dispersion region, we were able to unambiguously observe MI sidebands for k values ranging from −2 to 2. Measured MI peaks are depicted by markers in Fig. 4 and are in excellent agreement with the QPM curves obtained from Eq. (3). This equation predicts the position of phase matched frequencies but does not provide any information about their gain. Thus, a perfect phase matching can exist without an amplification process occurring. This could explain why we were not able to observe experimentally all the solutions predicted by Eq. (3), such as the second branch of solutions for $k = +2$ for instance (see Fig. 4).

Typical spectra are displayed in Figs. 5(a) and 5(b). The pump component has been cut in order to clearly see the MI sidebands whose intensity is 50 dB or more below the pump. Figure 5(a) focuses on $k \leq 0$ values. It shows the MI spectrum obtained for a 1057.7 nm pump, corresponding to a $\bar{\beta}_2$ value of 0.13 ps^2/km (normal average dispersion). It highlights the generation of $k = 0$; −1; −2 sideband pairs, respectively, in orange, green, and purple lines. Orange peaks correspond to $k = 0$ and therefore originate from the FOD term alone. They correspond to the same MI solutions as the one observed in uniform fibers [1,2].

MI sidebands displayed in green and purple (corresponding to k values of −1 and −2, respectively) arise from a combination of the FOD and of the periodic dispersion map. Indeed, the $\bar{\beta}_4$ term allows for these higher-order MI modes ($k < 0$) to exist while pumping in the normal dispersion region, similarly to the $k = 0$ case. Note that the peaks depicted in black correspond to Stokes and anti-Stokes stimulated Raman scattering (SRS) bands. Figure 5(b) focuses on $k > 0$ values. It shows the simultaneous generation of two sideband pairs (in red lines, with arrows pointing to them) by increasing the $\bar{\beta}_2$ value to 0.49 ps^2/km (corresponding to a

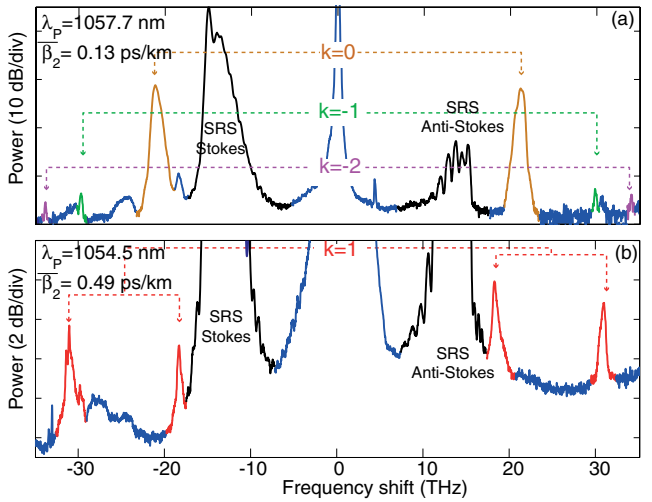

Fig. 5. Experimental spectra corresponding, respectively, to 1057.7 and 1054.5 nm pump wavelengths.

1054.5 nm pump wavelength). This feature is slightly different from the previous one in the sense that it is responsible for the generation of a second set of solutions for a given average dispersion (the ones with the largest frequency shifts from the pump, see Fig. 4). As a consequence, this new family of unstable MI frequencies is a unique feature of DOFs when higher-order dispersion terms are accounted for.

In summary, we have demonstrated that FOD can play an important role on the MI process in DOFs. This additional term leads to two different behaviors, one similar to the one observed in uniform fibers leading to the generation of MI sidelobes, whatever the sign of dispersion (provided $\bar{\beta}_4 < 0$), and a second one that is specific to DOFs. It corresponds to the generation of a new family of MI frequencies arising from a combination of FOD and longitudinal periodic dispersion. Our experimental results are confirmed by a relatively simple theoretical analysis based on a QPM process.

This work was partially supported by the French Ministry of Higher Education and Research, the Nord-Pas de Calais Regional Council, and FEDER through the "Contrat de Projets Etat Région (CPER) 2007–2013," and the "Campus Intelligence Ambiante" (CIA). A. A. and F. B. acknowledge the support of the German Max Planck Society for the Advancement of Science.

References

1. S. Pitois and G. Millot, Opt. Commun. **226**, 415 (2003).
2. J. D. Harvey, R. Leonhardt, S. Coen, G. K. L. Wong, J. C. Knight, W. J. Wadsworth, and P. St. J. Russell, Opt. Lett. **28**, 2225 (2003).
3. S. Coen and M. Haelterman, Phys. Rev. Lett. **79**, 4139 (1997).
4. F. Matera, A. Mecozzi, M. Romagnoli, and M. Settembre, Opt. Lett. **18**, 1499 (1993).
5. K. Kikuchi, C. Lorattanasane, F. Futami, and S. Kaneko, IEEE Photon. Techol. Lett. **7**, 1378 (1995).
6. N. J. Smith and N. J. Doran, Opt. Lett. **21**, 570 (1996).
7. P. Kaewplung, T. Angkaew, and K. Kikuchi, IEEE J. Lightwave Technol. **20**, 1895 (2002).
8. M. Droques, A. Kudlinski, G. Bouwmans, G. Martinelli, and A. Mussot, Opt. Lett. **37**, 4832 (2012).
9. S. Ambomo, C. M. Ngabireng, P. T. Dinda, A. Labruyere, K. Porsezian, and B. Kalithasan, J. Opt. Soc. Am. B **25**, 425 (2008).
10. M. Droques, A. Kudlinski, G. Bouwmans, G. Martinelli, and A. Mussot, Phys. Rev. A **87**, 013813 (2013).
11. S. G. Murdoch, R. Leonhardt, J. D. Harvey, and T. A. B. Kennedy, J. Opt. Soc. Am. B **14**, 1816 (1997).
12. F. K. Abdullaev and J. Garnier, Phys. Rev. E **60**, 1042 (1999).
13. A. Armaroli and F. Biancalana, Opt. Express **20**, 25096 (2012).
14. S. G. Murdoch, M. D. Thomson, R. Leonhardt, and J. D. Harvey, Opt. Lett. **22**, 682 (1997).
15. J. A. Sanders, F. Verhulst, and J. Murdock, *Averaging Methods in Nonlinear Dynamical Systems* (Springer, 2010).
16. M. E. Marhic and F. S. Yang, J. Lightwave Technol. **17**, 210 (1999).
17. M. Farahmand and M. de Sterke, Opt. Express **12**, 136 (2004).